Coastal Engineering 56 (2009) 332–340

Contents lists available at ScienceDirect

Coastal Engineering

journal homepage: www.elsevier.com/locate/coastaleng

Laboratory and numerical studies of wave damping by emergent and near-emergent wetland vegetation

Lauren N. Augustin [a], Jennifer L. Irish [b,*], Patrick Lynett [b]

[a] HDR Shiner Moseley, 555 N. Carancahua, Suite 1650, Corpus Christi, TX 78478 USA
[b] Coastal and Ocean Engineering Division, Zachry Department of Civil Engineering, Texas A&M University, College Station, TX 77843-3136 USA

ARTICLE INFO

Article history:
Received 29 February 2008
Received in revised form 25 June 2008
Accepted 11 September 2008
Available online 31 October 2008

Keywords:
Wave attenuation
Vegetation damping
Bottom friction
Wetlands

ABSTRACT

Wetlands protect mainland areas from erosion and damage by damping waves. Yet, this critical role of wetland is not fully understood at present, and a means for reliably determining wave damping by vegetation in engineering practice is not yet available. Laboratory experiments were conducted to measure wave attenuation resulting from synthetic emergent and nearly emergent wetland vegetation under a range of wave conditions and plant stem densities. The laboratory data were analyzed using linear wave theory to quantify bulk drag coefficients and with a nonlinear Boussinesq model to determine numerical friction factors to better represent wetland vegetation in engineering analysis.

1. Introduction

The latest trends in coastal engineering are focusing on more non-intrusive forms of shore protection such as vegetation, which protects the shoreline and provides a natural habitat for many different species of fish, amphibians, shellfish, insects, and birds. Aquatic vegetation helps regulate water levels, improve water quality, reduce flood and storm damages, provide important fish and wildlife habitats, and support recreational activities. Additionally, vegetation directly increases the durability of shorelines through the root systems and enhances the storage of sand in dunes (Dean, 1978). Until recently the importance and function of wetlands was not well understood, and the area of wetlands being degraded and lost annually in the United States alone was approximately 300 to 400 km^2 (Environmental Protection Agency, 2007).

Extreme weather events and projected sea level rise has led to increasing interest and research in wave attenuation due to coastal vegetation. It is commonly known that vegetation dissipates energy and aids in shoreline protection by damping incoming waves and depositing sediment in vegetated regions. While bottom characteristics in general are important when determining wave damping, wetland ecosystems are among one of the more important particularly because the impact on hydrodynamics is realized not only at the bottom but throughout the water column. Therefore, the interaction between water waves and vegetation needs to be quantified (Asano et al., 1992).

Friction dissipation due to vegetation elements is commonly accounted for by a roughness coefficient, such as the Manning coefficient or by applying the dimensionless Darcy friction factor. The bottom roughness coefficients for predicting energy dissipation due to the presence of vegetation are an important parameter in storm wave and surge models as well as for river and estuary mixing and transport models. Unfortunately, studies to quantify a wave friction factor due to vegetation are very limited.

The purpose of this paper is to present an engineering approach for quantifying the impacts of commonly-occurring coastal wetlands on the wave field using existing wave models. In this paper, wave attenuation has been investigated through laboratory measurements and an empirical equation is derived to estimate a friction factor under waves due to the presence of both emergent, most widely found in marsh systems, and near-emergent vegetation for a range of horizontal stem spacing densities. The numerical model COULWAVE (Cornell University Long and Intermediate Wave Model; Lynett et al., 2002), based on the modified Boussinesq equations, is used to calibrate a friction factor from the collected data for each of the laboratory experiments. In the following sections we will discuss background literature relevant to wave attenuation and vegetation roughness formulations, outline the experimental setup, present laboratory results quantitatively and formulate a set of equations for a numerical friction factor calibrated using the COULWAVE model.

2. Theoretical background

It is well-accepted that wave attenuation by emergent and submerged vegetation is a function of plant characteristics (geometry, stem

* Corresponding author. Tel.: +1 979 845 4586; fax: +1 979 862 8162.
E-mail address: jirish@civil.tamu.edu (J.L. Irish).

0378-3839/$ – see front matter © 2008 Elsevier B.V. All rights reserved.
doi:10.1016/j.coastaleng.2008.09.004

density, spatial coverage, buoyancy, stiffness) as well as hydrodynamic conditions including water depth (h), wave period (T) and wave height (H) (Fig. 1). In addition, relative depth of plant submergence as indicated by the ratio between water depth and submerged plant stem height (l_s), has been shown to strongly influence the vertical velocity profile behavior under steady flow conditions (Nepf, 2004), and it is anticipated that depth of submergence is also important in wave attenuation by vegetation. Here we adopt the following three flow condition definitions which are similar to those of Nepf (2004): emergent where h/l_s is equal to 1, near-emergent where h/l_s is between 1 and 2, and deeply submerged where h/l_s is greater than 10. For discussion purposes, we introduce a fourth flow condition: transitional submerged where h/l_s is between 2 and 10.

In general, the damping of surface waves is caused by the energy loss through work performed on the plants (Mork, 1996), and numerous models exist that attempt to relate the interactions between waves and submerged vegetative plants to explain the damping effects of vegetative fields. Interaction of fluid flow in aquatic vegetation is unsteady because the structure of the plant field changes with time as it is exposed to the physical forcing of wave action and water flow (Mendez and Losada, 2004). The first hydrodynamic model developed by Price et al. (1968) simulated the effects of submerged seaweed as a high viscous layer. Mork (1996) extended the idea of the high viscous layer and developed a theory for kelp plants that took into account not only viscous drag, but form drag for the canopy layer and the lower vegetative area. Vegetation has also been modeled as a high friction area by Camfield (1983) who studied wind–wave growth over shallow flooded regions. Numerous models predict wave attenuation using the conservation of wave energy equation and account for vegetation effects in an energy dissipation term (Dalrymple et al., 1984; Mendez and Losada, 2004) while others use the conservation of momentum approach (Kobayashi et al., 1993; Lima et al., 2006). Mendez et al. (1999) extended the previous momentum-based wave damping theories developed by Kobayashi et al. (1993) and Dubi and Torum (1995) to include random waves. Both approaches represent vegetative resistance as a drag force and all of these methods ultimately derive a solution for the decay in wave energy through the vegetation field as a function of wave height, H. The general equation for wave height decay is given by:

$$K_v(x) = \frac{H(x)}{H_o} \tag{1}$$

where K_v is the wave transmission coefficient as a function of distance through the plant bed and H_o is the approaching wave height. Kobayashi et al. (1993) assumed wave height decayed exponentially with distance of propagation through the plant field. Energy dissipation when linear wave theory is applied to the conservation of energy equation gives (Dalrymple et al., 1984):

$$K_v(x) = \frac{1}{\left\{\left[\frac{g^2 C_D N d H_o}{9\pi c_G c^3}\frac{(\cosh^3 kl_s + 2)\sinh kl_s}{\cosh^3 kh}\right]x + 1\right\}} \tag{2}$$

where

C_D is drag coefficient for an individual plant stem
$N = 1/\Delta S^2$ is stem density, or number of plant stems per unit bottom area, where ΔS is stem spacing
d is plant stem diameter
k is wavenumber
c_G is wave group speed
c is wave phase speed

Unfortunately, the variety of wetland plants is extensive and trying to find a generalized method for modeling the behavior of plant dissipation for practical application is difficult (Mendez and Losada, 2004). The majority of vegetated hydrodynamics studies have focused on submerged vegetation (e.g., those wave attenuation studies mentioned above). The objectives of this research are to investigate in the laboratory attenuation by vegetation during emergent and near-emergent conditions with emphasis on understanding the influence of different wave and vegetation parameters on wave height decay and to quantify bulk friction properties during emergent and near-emergent conditions for practical wetlands application.

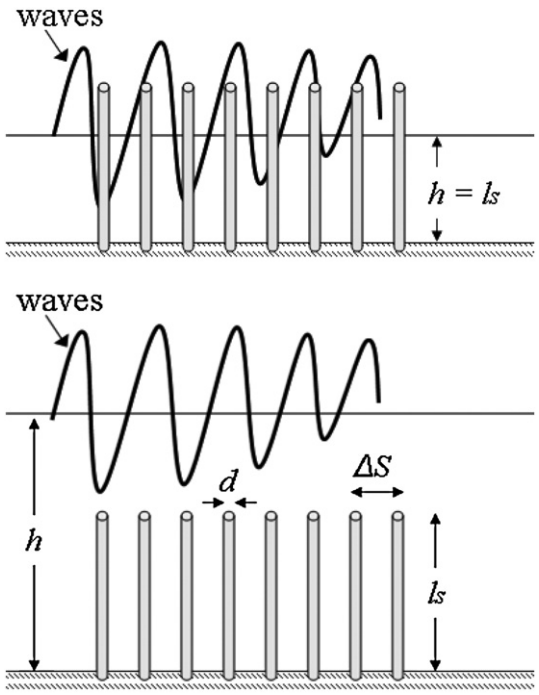

Fig. 1. Definition sketch of typical vegetation model (h is depth, d is stem diameter, l_s is submerged stem height, and ΔS is stem spacing). Top pane is emergent conditions and bottom pane is near-emergent ($h<2l_s$) submerged conditions. Modified from Nepf (2004) and Dean and Bender (2006).

3. Bottom roughness coefficient formulation

Vegetation is one of the main factors influencing hydraulic roughness, with other factors being sediment grain size, bottom bathymetry, sediment transport, and flow obstructions. Both the Manning and Darcy–Weisbach open channel flow equations have been successfully applied to flows in the presence of vegetation in the field and in the laboratory. The Manning's equation in SI units is given by:

$$\frac{Q}{A_c} = \overline{u} = \frac{1}{n} R_h^{2/3} S^{1/2} \tag{3}$$

where n is the Manning's roughness factor in units of s/m$^{1/3}$, R_h is the hydraulic radius, and S is the slope of the water surface. The Darcy–Weisbach equation originally developed for pipe flow theory is expressed as:

$$\overline{u}^2 = \frac{8 g R_h S}{f} \tag{4}$$

where f is the non-dimensional Darcy–Weisbach friction factor. Both the Darcy friction factor for pipe flow, f, and Manning coefficient, n, relate the wall shear stress to the material of the bounding surface (Munson et al., 2002), therefore there are various relationships

available that describe n in terms of the Darcy friction factor, f. For a wide shallow channel, the relationship in metric units between Manning's n and the Darcy friction factor f is given by:

$$n = \sqrt{f\left(\frac{h^{1/3}}{8g}\right)} \tag{5}$$

According to Kadlec (1990) the Manning equation assumes that flow is fully turbulent, which is usually not the case in wetland flow areas during daily conditions; however, during storm conditions both wave-driven and surge-driven flows are likely to be turbulent. Many studies have found that the Manning coefficient is strongly dependent on factors including the depth, vegetation density, and Reynolds number. The Darcy–Weisbach approach is suitable for flows that range from laminar to turbulent flow, but is also dependent on various parameters such as depth, Reynolds number and vegetation type (Kadlec, 1990). Despite the assumption of turbulent flow, the Manning equation is the most widely used in practice.

The Darcy–Weisbach friction factor was originally developed for steady pipe flow, and is not designed to represent bottom friction in unsteady turbulent boundary layers that are present under waves. There have been numerous relationships derived relating the friction factor to different flow regime boundary layers to attempt to derive a wave friction factor for estimating energy dissipation due to bottom bed roughness. The boundary layer problem is fairly complex, and studies relating the wave friction factor to vegetation roughness elements are sparse. Here, we adopt a friction factor approach in the numerical analysis such that the friction factor approximately equates with the bulk drag coefficient (C_D') representing the average drag force per unit width across the wave propagation direction:

$$C_D' = C_D\left(\frac{l_s d}{\Delta S h}\right) \tag{6}$$

where C_D is the individual plant stem drag coefficient and ΔS is stem spacing. As discussed in the following sections, friction factor will be determined through numerical model calibration using the experimental data.

Existing numerical models currently lack a robust capability to quantify wave attenuation in the presence of wetland vegetation. In this research, experimental data are analyzed using linear wave theory and nonlinear Boussinesq theory to determine an appropriate friction factor for numerical applications in order to estimate the energy dissipation under waves when plants are emergent and near-emergent. The friction factors determined through the model comparisons with the collected data were used to develop a set of empirical equations to estimate wave friction factors for both emergent and near-emergent conditions. The empirical relationships presented herein may readily be used in practical numerical applications to determine wave attenuation through wetland vegetation as it relates to water quality and mixing, coastal erosion, and storm damage.

4. Experimental setup

The species *Spartina alterniflora* is one of the most prevalent low marsh wetland grasses. *S. alterniflora* have relatively stiff, reed-like stems on the order of 10 mm in diameter and 30 to 240 cm in height (Tiner, 1993; U.S. Department of Agriculture, 2008); average stem density (N) for *S. alterniflora* fields are reported to be between 100 and 600 stems/m^2 (Bergen et al., 2000; Tyler and Zieman, 1999). Our experimental layout was design to approximate a range of *S. alterniflora* plant field configurations.

Experiments were conducted in a wide wave flume constructed in the Haynes Coastal Engineering Laboratory shallow-water wave basin and in the narrow wave flume at Texas A&M University to assess the effects of water depth, wave period, and stem density (N) on wave attenuation through synthetic plant fields. Both rigid elements constructed out of cylindrical wooden dowels and flexible elements constructed out of polyethylene foam tubing were analyzed. The diameter, material density, and tensile strength of the polyethelene foam were 12 mm, 32 kg/m^3, and 344.7 kPa, respectively. The diameter of the wooden dowels was also 12 mm in order to compare the effects of rigid versus flexible plant type. Mechanical properties, namely rigidity and density, of both flexible and rigid stem elements are similar to those of *S. alterniflora* plant stems (Feagin, 2008, personal communications). Stems were held constant at a length (l_s) of 0.3 m for all laboratory experiments. Control runs were conducted prior to the experimentation with synthetic vegetation fields, and all experiments were completed twice to ensure they were repeatable and accurate representations of the conditions being tested.

Tests conducted in the narrow wave flume were used to investigate the effects of plant stem rigidity and stem density on attenuation of monochromatic waves under emergent and near-emergent conditions. This laboratory flume is 30.5 m long, 0.9 m wide, and 1.2 m deep. A SEASIM (RSW 90-85) Rolling Seal absorbing paddle wave maker was used for generating waves at one end of the flume and a 3 m long rubber horsehair beach was constructed at the opposite end to absorb wave energy and reduce reflection effects (Fig. 2). The vegetation field was placed approximately 13.1 m from the wave maker and extended 6 m down the length of the tank. Five resistance wire probe electronic wave gages were used to measure the free surface oscillations in the vegetation field for each test run. The gages were spaced equally 1.5 m apart from the beginning to the end of the field, and free surface elevation was recorded by each wave probe at a sampling rate of 25 Hz.

Three different test scenarios were attempted using rigid and flexible vegetation elements. The first experiment consisted of a flexible polyethylene foam vegetation field with a stem spacing of $\Delta S = 10.2$ cm corresponding to a stem density of $N = 97$ stems/m^2 (Fig. 3) and was selected to minimize sheltering effects (Nepf, 2004) in order to simplify the problem for initial study. For the second set of experiments the stem density was doubled to $N = 194$ stems/m^2 by placing a stem in the center of each 10.2-cm^2 (Fig. 3); this stem density corresponds with a stem spacing of $\Delta S = 7.2$ cm. The third vegetative

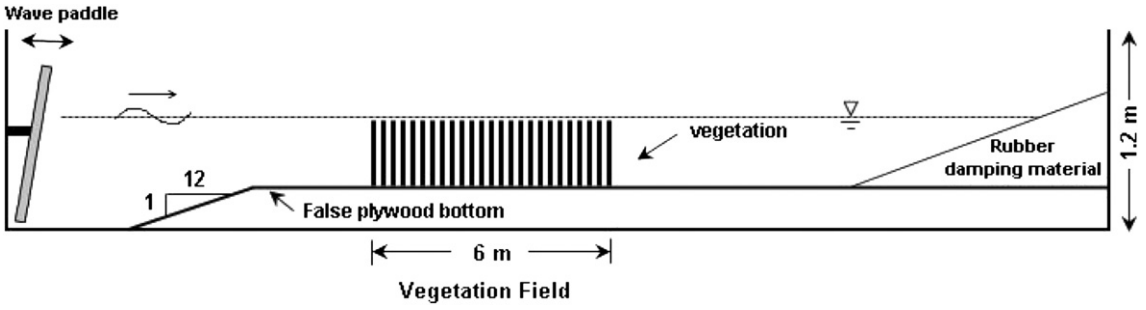

Fig. 2. Schematic of narrow wave flume setup.

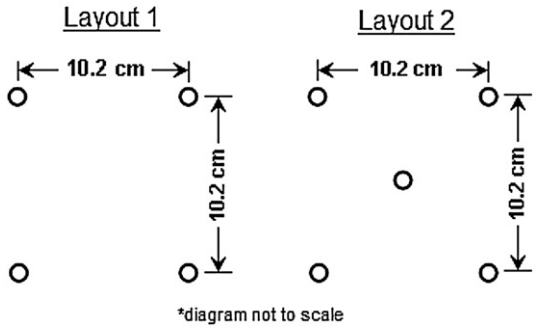

Fig. 3. Schematic of synthetic vegetation stem configurations. Left pane is stem density of N=97 stems/m^2 and right pane is stem density of N=194 stems/m^2.

scenario was constructed out of rigid cylindrical dowels using the higher stem density layout.

Experiments conducted in the shallow-water wave basin investigated irregular waves over flexible vegetation to determine the effect of stem density for both emergent and near-emergent plant conditions. The basin dimensions are 22.9 m wide by 30.5 m long and 1.2 m deep. A 42 paddle fully programmable, directional wave maker was located at one end for wave generation, and a rock beach approximately 3 m long was located at the opposite end for energy absorption. For this portion of the investigation a 4.6-m wide flume was constructed along one side of the basin and enclosed with large concrete blocks (Fig. 4). Reflection was minimized by using the wave maker's active energy absorption setting. Six wireless capacitance wave gages were used for free surface displacement time series collection. The irregular waves were sampled at 25 Hz and collected over a duration of 1200 s to ensure a long enough wave record for accurate spectral analysis.

The synthetic vegetation field measuring 6 m long and 4.6 m wide and with a stem spacing of ΔS=10.2 cm corresponding to a stem density of N=97 stems/m^2 (Fig. 3) was placed near the center of the wide basin flume (Fig. 4). A TMA shallow-water wave spectrum was used for generating each irregular wave test. The target spectral wave height was held constant, while the peak period and water depth were varied for analysis.

In addition to the series of tests conducted on the homogeneous vegetation field, to investigate the impact of vegetation field heterogeneity on wave attenuation a set of experiments were conducted where stem density in the front-center vegetation field section measuring 1.5 m wide by 3 m long was increased to N=194 stems/m^2 corresponding with a stem spacing of ΔS=7.2 cm (Fig. 4).

Incident wave height, wave period, and water depth were varied during both the wide and narrow wave flume experimental runs to quantitatively analyze the effect of each forcing parameter on wave damping. Wave periods representative of nearshore wind waves were chosen for testing, which ranged from 1.5 to 2.0 s. Additionally, two separate depths were analyzed, the first with the vegetation under emergent conditions (h=0.3 m), which is most prevalent in marshes during regular tidal conditions, and the other with the vegetation under near-emergent conditions (h=0.4 m), resulting in a depth to stem height ratio of h/l_s=1.33. The water depths and wave periods analyzed were equivalent in both the basin and flume experiments for experiment similarity. Thirty-three test cases with vegetation were conducted in the narrow flume while 13 test cases with vegetation were conducted in the wide flume.

5. Experimental results

The experimental data were analyzed to determine wave attenuation by the vegetation field and to estimate drag properties. To determine wave statistics for each experimental test using monochromatic waves in the narrow flume, a wave-by-wave analysis using the zero-upcrossing method was performed on each free surface time series measured in the wave flume. The root-mean-square wave height (H_{rms}) and mean wave period were determined for each of the five probe points in the vegetation field.

For the wide flume experiments using irregular waves, spectral wave characteristics were obtained from each of the water elevation time series by Fourier-based analysis. The spectral wave height, H_{m0}, value was calculated from the total energy in the spectrum and was assumed to be approximately equal to the significant wave height, $H_{1/3}$. Wave period at the spectral peak was also determined. For data comparison with the monochromatic experimental data, the spectral moment wave heights were converted to the root-mean-square wave height by assuming a Rayleigh distribution, using the relation:

$$H_{1/3} = H_{m0} = 1.416 H_{rms} \tag{7}$$

In order to isolate the influence of vegetation on wave attenuation, background attenuation losses as measured during control tests were removed. Here, the attenuation due to vegetation only is expressed in terms of the vegetation transmission coefficient, K_v (Eq. (1)), and is given by:

$$K_v = K_t + (1 - K_b) \tag{8}$$

where K_t is the total measured wave decay and K_b is the decay resulting from frictional effects due to presence of the bottom and side

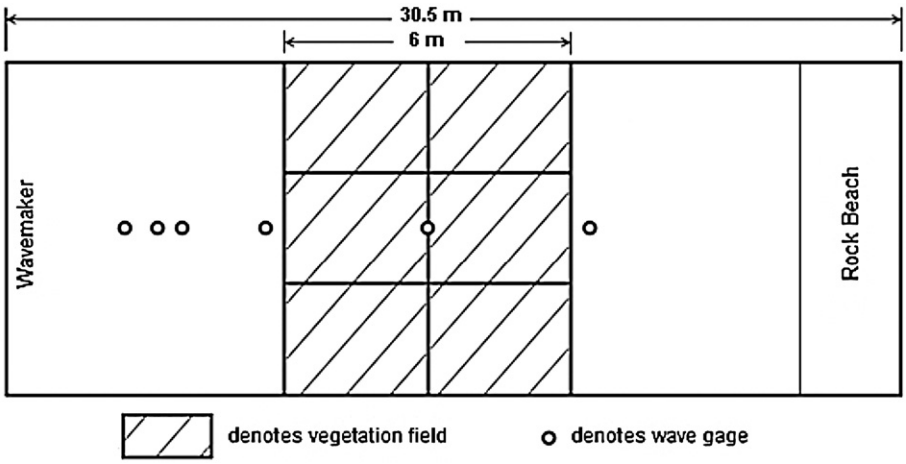

Fig. 4. Plan view of vegetation field setup inside wide flume in shallow-water wave basin at Haynes Coastal Engineering Laboratory. Double-hatched area indicates location of high-density vegetation during heterogeneous test conditions.

walls of the flume. Data collected during unvegetated control experiments were used to ascertain K_b. The experimental data showed that wave attenuation under emergent conditions is 50 to 200% greater per wavelength than attenuation under near-emergent conditions, for the same plant field configuration and wave condition. In wave propagation through emergent vegetation drag effects are distributed throughout the water column; therefore wave velocities are impacted along the entire vertical velocity profile. In contrast, during the near-emergent experiments a portion of the water column was unobstructed by the plant stems and allowed to flow freely, resulting in less wave damping in comparison to that during emergent conditions.

Using Eq. (2), the individual plant stem drag coefficient, C_D, was computed for each experimental measurement. Fig. 5 (top pane) presents C_D versus Reynolds number (Re):

$$Re = \frac{u_{max} d}{\nu} \tag{9}$$

where ν is the dynamic viscosity of water, d is stem diameter, and u_{max} is the maximum horizontal orbital velocity associated with H_{rms} as given by linear theory at the measurement location. This figure indicates that under emergent conditions the drag coefficient decreases as the waves decay ($u_{max} \propto H$) thereby slowing wave attenuation. In this regime the correlation coefficient between Re and C_D is around 0.75 for all cases. In contrast, the correlation between Re and C_D under near-emergent conditions is weak yielding correlation coefficients around 0.26. Mendez and Losada (2004) showed that for very flexible vegetation (kelp) under transitional submerged conditions (defined here as $10 \geq h/l_s \geq 2$ and is the regime between the near-emergent and deeply submerged regimes suggested by Nepf (2004)) the drag coefficient was much more highly correlated with the Keulegan–Carpenter number ($KC = u_{max}T/d$) than with the Reynolds number. While not nearly as well-correlated as the data presented by Mendez and Losada (2004), our data also demonstrate a somewhat better correlation between KC and C_D for the near-emergent cases (Fig. 5, bottom pane) yielding correlation coefficients around 0.43. However, under emergent conditions KC and C_D are not well-correlated, with correlation coefficients around 0.28. This suggests that the dependence of C_D on wave period (T) increases with increasing h/l_s as the regime changes from emergent to near-emergent to transitional submerged.

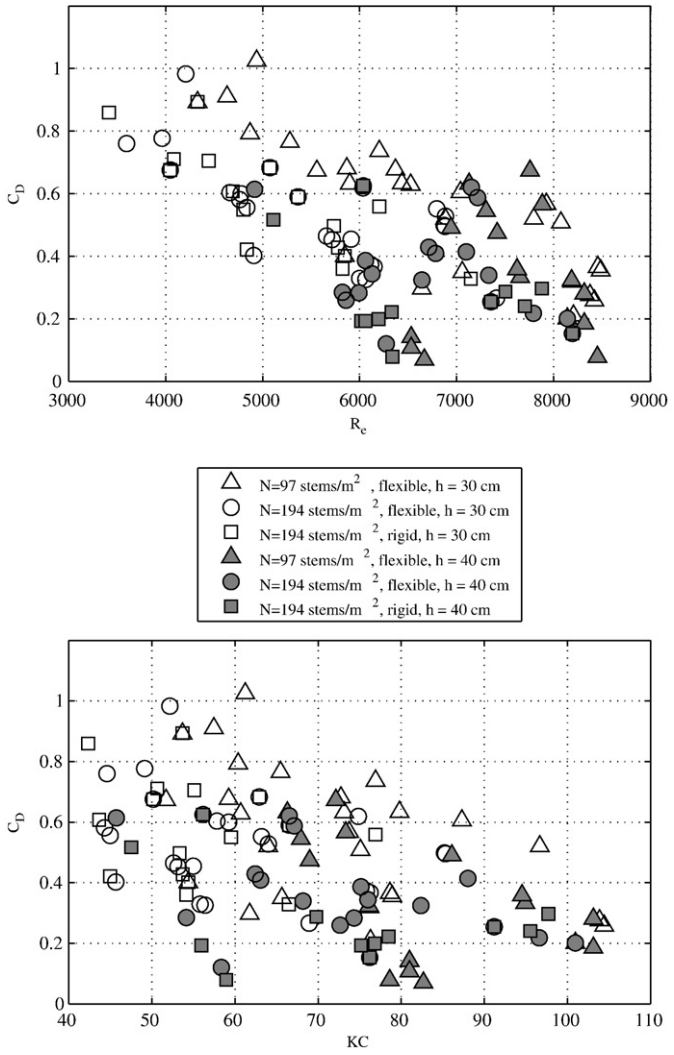

Fig. 5. Measured individual plant stem drag coefficient (C_D) versus Reynolds number (Re, top pane) and Keulegan–Carpenter number (KC; bottom pane) computed locally at each measurement location.

Also seen in Fig. 5 is the relative influence of stem density (N). In general, the lower plant stem density cases yield higher C_D values than the higher plant stem density cases. This is most likely an artifact of sheltering between individual plant stems such that the effective velocity acting on an individual stem at higher plant stem densities is somewhat lower than that on an unsheltered stem. The experimental data also indicate that stem density has more impact on wave attenuation under emergent conditions than under near-emergent conditions, especially within the first wavelength of propagation.

Finally, Fig. 5 shows little difference between attenuation, and C_D, by flexible and rigid plant elements within the range of flexibilities tested. It should be noted, that while swaying back and forth of the flexible stems as waves passed was observed during testing at no time were the flexible elements moved more than about 20° from vertical.

An effective, bulk drag coefficient (C_D', see Eq. (6)) representing the average drag force per unit width across the wave propagation direction lends itself well to numerical modeling applications as will be discussed below. Under near-emergent and emergent conditions, measured average C_D' ranges from 0.01 to 0.08 and 0.05 to 0.15, respectively.

5.1. Heterogeneous effects

Data collected during heterogeneous vegetation field experiments are presented in Table 1. In this table, the energy attenuation for the first 3 m and last 3 m of wave propagation through the vegetation field are presented, in addition to the total percent wave height decay. With uniform stem density, the energy attenuation appears to be fairly uniform over the vegetation field. A higher amount of energy was dissipated in the first half of the plant bed in experiments where the initial 3 m of the vegetation was more dense ($N = 194$ stems/m^2). This is expected not only due to the increase in stem density causing more frictional drag, but also because the wave height entering the last 3 m is characterized by a lower fluid velocity which results in a reduction of drag on the plant stems in this region.

The C_D for the each homogenous section making up the two center panels of the heterogeneous vegetation field were computed using Eq. (2). The resulting values, included in Fig. 5, are consistent with C_D computed for the homogeneous cases. This finding implies that application of friction factors determined for homogeneous vegetation fields may be applied in a patchwork manner to quantify wave attenuation in a heterogeneous vegetation field.

6. Numerical analysis

Most research on wave attenuation by vegetation has focused on the application of linear wave theory. This study provides one of the first attempts to derive a general formulation for a determining a

Table 1
Percent energy loss through first 3 m and last 3 m of heterogeneous vegetation field (see Fig. 4 for layout)

H_{rms} (cm)	T (s)	h (m)	N (stems/m^2)	Percent wave height reduction		
				0–3 m	3–6 m	0–6 m
8.5	2.0	0.3	97	14.7%	14.9%	29.6%
8.5	2.0	0.3	194/97*	24.9%	7.9%	32.8%
8.5	2.0	0.4	97	11.5%	8.8%	20.3%
8.5	2.0	0.4	194/97*	18.4%	5.7%	24.1%
8.5	1.5	0.3	97	17.6%	14.6%	32.2%
8.5	1.5	0.3	194/97*	29.4%	11.8%	41.2%
8.5	1.5	0.4	97	10.1%	17.4%	27.5%
8.5	1.5	0.4	194/97*	16.3%	5.0%	21.3%

*Higher density in first 3 m while lower density in last 3 m.

friction factor for wetland plants species to predict wave damping due to vegetation roughness using nonlinear wave theory. The experimental conditions tested here have wave height to water depth ratios ranging from 0.2 to 0.4. Various publications classify these waves as both weak and strong nonlinear waves, although the authors would consider them here to be weakly nonlinear. The numerical model COULWAVE was applied to simulate the physical experiments conducted in the basin and the flume. COULWAVE (Lynett et al., 2002) is based on the modified Boussinesq equations and simulates wave propagation from intermediate to shallow-water depths. The fundamental assumption of this depth-integrated model is that the ratio of the wavelength to water depth is large. However, the Boussinesq type equations are known to be accurate from fairly deep water to the shoreline (Wei et al., 1995), and have been shown to give good predictions of field data (Elgar and Guza, 1985) and laboratory data (Goring, 1978; Liu et al., 1985), as long as the frequency dispersion and nonlinear effects are weak. The governing equations of the model are derived from the Navier–Stokes equations for the conservation of momentum and conservation of mass in fluid flow. The leading order terms in the Boussinesq governing equations are:

$$\partial\eta/\partial t + \nabla\cdot[(h+\eta)\boldsymbol{u}_\alpha] + \text{H.O.T.} = 0 \tag{10a}$$

$$\partial\boldsymbol{u}_\alpha/\partial t + \boldsymbol{u}_\alpha\cdot\nabla\boldsymbol{u}_\alpha + g\nabla\eta + \text{H.O.T.} + R_b = 0 \tag{10b}$$

Where $\boldsymbol{u}_\alpha$ is the horizontal velocity vector evaluated at a reference level, η is the free surface elevation, H.O.T. represents the numerous dispersive terms characteristic of the Boussinesq model (e.g. see Lynett et al., 2002), and R_b is a frictional dissipation term to be described below. The COULWAVE model was applied here to determine a representative friction factor for each laboratory vegetation experiment. Frictional effects were calculated using the quadratic term R_b expressed as:

$$R_b = f\frac{\boldsymbol{u}_b|\boldsymbol{u}_b|}{h+\eta} \tag{11}$$

Where $\boldsymbol{u}_b$ is the instantaneous horizontal wave orbital velocity vector at the bed and f is the non-dimensional Darcy friction factor.

The model was modified to agree with the characteristics of the physical setup in each laboratory configuration. COULWAVE was adjusted to allow for propagation of two-dimensional waves over a distance of 30.5 m, equal to the length of both laboratory facilities. The model analysis was divided up into two parts in order to model the basin and flume, and simulated all laboratory experiments, including both irregular and monochromatic wave conditions. A quadratic friction factor was used to model the vegetation roughness along the length of the vegetation field (Eq. (11)). A friction factor of 0.001, a typical value for smooth surfaces, was specified for areas outside the vegetation field to account for the reduced energy dissipation due to the wave flumes' smooth bottom and side walls. Each model simulation was run for a duration of 200 s (100–133 wave periods). COULWAVE incorporates a numerical 'sponge layer' at the end of the grid that absorbs all energy at the end of the flume, thereby removing reflection from the numerical simulation. Example numerical free surface snapshots are shown in Fig. 6. To understand the spatial variation as the waves propagate through the model, a plot of the free surface elevation as a function of distance is shown below in Fig. 6a for the wide channel (irregular waves) and b for the narrow channel (regular waves). It can be seen that the wave height is dampened over the vegetation region beginning at the 13.1 m point, extending 6 m to the end of the field at 19.1 m.

The friction factor was determined for each experimental case through an iterative process. A final friction factor value for each experimental test was chosen based on a best-fit between the simulated and total amount of measured energy dissipation through the entire vegetation field. An example of the modeled friction factor versus the measured experimental data for submerged (Fig. 7a) and emergent (Fig. 7b) plant conditions. Submerged conditions showed a better fit to the numerical simulation because the roughness elements are not occupying the entire water column, and are therefore a more reasonably represented by a roughness coefficient at the sea bottom. This is also an indication that the quadratic dissipation term with a time-constant friction coefficient may not be entirely suitable for modeling the time evolution of wave height through the highly-dissipative, emergent vegetation.

Due to the large number of experiments, the friction factor is presented graphically. The friction factor for all experimental cases, including emergent and submerged plant conditions, is plotted

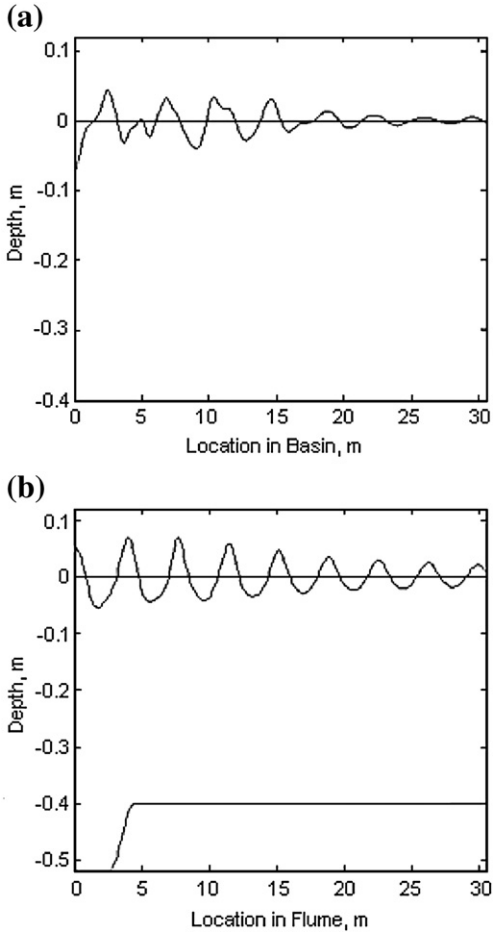

Fig. 6. Simulated free surface elevation as a function of distance for (a) irregular waves in basin (b) monochromatic waves in flume. The vegetation region in both plots stretches from $x = 13.1$ m to $x = 19.1$ m. The bottom line in pane (b) indicates the bottom elevation within the flume.

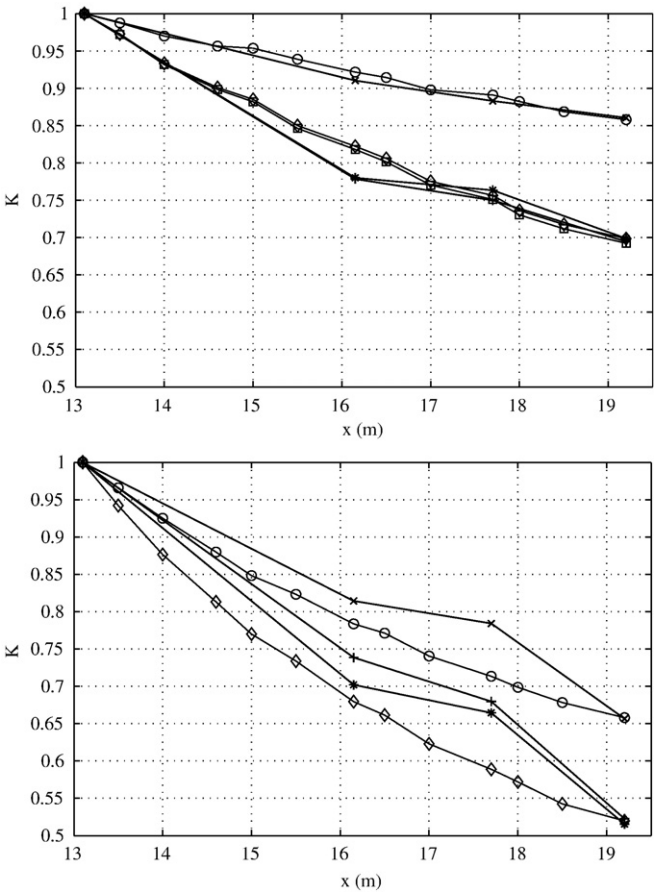

Fig. 7. Collected laboratory measurements versus numerical friction factor for near-emergent conditions when H_i=12 cm, T=1.5 s and h=0.4 m (top pane) and for emergent conditions when H_i=9 cm, T=1.5 s, and h=0.3 m (bottom pane). The ×, +, and * symbols represent measured data for flexible stems with N=97 stems/m^2, flexible stems with N=194 stems/m^2, and rigid stems with N=194 stems/m^2, respectively. The circles, diamonds, and squares in top pane represent simulated results with f_N=0.024, f_N=0.066, and f_N=0.068, respectively, while the circles and diamonds in bottom pane represent simulated results with f_N=0.083 and f_N=0.151, respectively.

against the dimensionless Ursell number in Fig. 8. The Ursell number is given by:

$$U_R = \frac{L^2 H}{h^3} \tag{12}$$

where L is wavelength. Here, Ursell number is computed by using root-mean-square wave height and peak wave period (mean period for monochromatic cases). Shallower water depths with greater periods yield higher Ursell numbers compared to deeper water depths. Fig. 8 shows that for submerged conditions the friction factor tends to increase with increasing Ursell number. The increasing trend shows the dependency of the friction factor value on water depth and wave period. Emergent conditions are fairly scattered, most likely due to the friction factor's dependence on other local flow conditions (i.e. Reynolds number). The values of friction factor increased for the higher plant density, but were not observed to depend on plant flexibility. The attenuation effects of the rigid and flexible vegetation elements appeared to be very similar and in some of the experimental cases yielded the same friction factor value. Overall, the same trends between Ursell number and friction factor are followed for all the experiments indicating that using an Ursell number dependent friction factor formulation will yield reasonable results. The average percent error for the regression lines is 16%. A larger percentage of error was observed for the regression lines fitted to submerged plant conditions. This is most likely due to influence of the ratio of stem length to water depth on wave damping, which is not accounted for in the friction factor formulation. The total average percent error for emergent regression lines was 10%. The findings from this research suggest that modeling vegetation roughness using a friction factor is a reasonable approximation for engineering applications.

A set of equations for each submergence condition (emergent [denoted with the superscript $^{(E)}$] and near-emergent [denoted with the superscript $^{(S)}$]) is formulated from the linear regression lines to estimate a wave friction factor for stem density values between 97 stems/m^2 and 194 stems/m^2. The numerically derived empirical wave friction factor equations for tested near-emergent ($f_N^{(S)}$) and emergent ($f_N^{(E)}$) plant conditions are as follows:

$$f_N^{(S)} = 0.002\left(1+\frac{N-97}{65}\right)U_R + 0.005\frac{(N-97)}{65} + 0.023 \tag{13a}$$

$$f_N^{(E)} = -7e{-}06\left(\frac{N-97}{65}\right)U_R + 0.059\frac{(N-97)}{65} + 0.085 \tag{13b}$$

where these relationships are valid when $97 \le N \le 194$ and $9.5 \le U_R \le 43.5$. These results are derived from experimental data collected using rigid and flexible plants with limited swaying motion and should be applicable for practical engineering purposes to wetland plant species such as *S. alterniflora* which have characteristics similar to the synthetic plant fields used during experimentation. For the case of unsteady hydrodynamic conditions Eqs. (13a,b) should be applied in a time-varying sense to account both for transition between emergent and near-emergent conditions and for changing incident wave conditions. However, plants that are extremely flexible (i.e., do not stand vertical on their own) are not valid in the above equations because a large amount of bending will result in a significantly lower friction factor than is predicted. Here, the friction factor becomes highly dependent on the Reynolds number when the velocity is high enough to bend the plant stems so that they are nearly parallel with the bed.

6.1. Heterogeneous vegetation simulations

With the above empirical equations for friction factor under submerged and emergent conditions, it is possible to construct a numerical simulation with a spatially variable friction factor, using the equation predictions for each region. Then, the numerical results can be compared with the experimental data for these heterogeneous cases. This exercise is meant to be a test of the derived friction factor

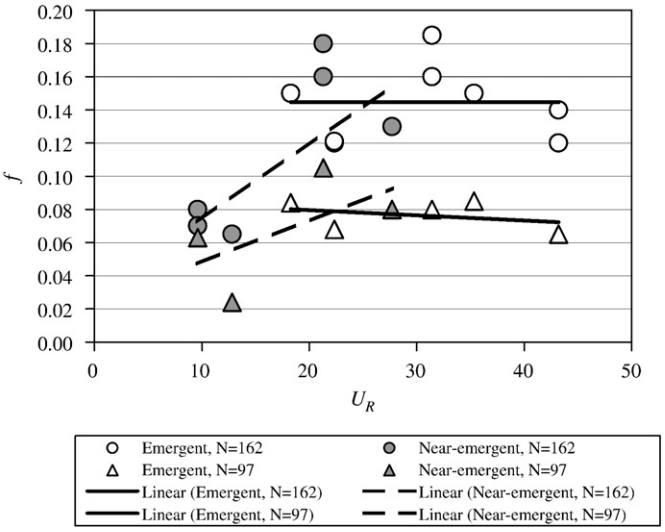

Fig. 8. Numerical friction factor versus Ursell number for emergent (h=0.3 m) and near-emergent (h=0.4 m) vegetation experiments.

Table 2
Comparison of experimental and numerical wave height reduction for the heterogeneous vegetation cases (see Fig. 4 for layout)

H_{rms} (cm)	T (s)	h (m)	N (stems/m^2)	U_R	f (N=194)	f (N=97)	Numerical wave height (H_N)/ Experimental wave height (H_E)	
							H_N/H_E after 3 m propagation	H_N/H_E after 6 m propagation
8.5	2.0	0.3	194/97*	33.4	0.145	0.085	0.93	1.04
8.5	2.0	0.4	194/97*	18.1	0.102	0.059	0.98	1.02
8.5	1.5	0.3	194/97*	17.3	0.146	0.085	0.91	1.02
8.5	1.5	0.4	194/97*	9.1	0.065	0.041	0.97	1.01

*Higher density in first 3 m while lower density in last 3 m.

equations, similar in principle to how they would be used in practice. Again, the heterogeneous vegetation experiments were performed in the wide channel, following the layout in Fig. 4, and are summarized in Table 1. The friction factors used in the numerical simulation are presented in Table 2.

A sample of the numerical results and data comparisons is given in Fig. 9. In the top subplot is the scaled RMS wave height along the centerline of the channel, and the lower plot shows the plan-view contours of scaled wave height predicted by the numerical model. From looking at the plan-view contours, clearly two-horizontal-dimension (2HD) effects play some role in the wave height. The higher frictional resistance of the front-center region causes the wave height to decrease at a faster rate than in the laterally neighboring regions. The cross-channel wave height gradient leads to cross-channel modes as the crest height attempts to reach equilibrium. This focusing of energy towards the center of the channel then leads to a lobe of locally higher wave height behind the vegetation patch. Note that this higher wave height lobe is due to the reflection off the side walls (i.e., tank effect) and would not necessarily be observed with real bathymetry except in cases of unique bathymetry (e.g., narrow channel). For the heterogeneous cases investigated here, the cross-channel variation of wave height varies between 0% and 10% of the centerline wave height.

The relative magnitude of this cross-channel variation can be seen clearly in the top plot of Fig. 9. In this plot are shown the numerically-predicted centerline wave height, the maximum predicted height through the channel, the minimum height, and the experimental data. Note that the centerline wave height coincides with the minimum wave height for $x<16$ m and with the maximum height for $x>16$ m. Also evident from this plot is that the numerical model is performing reasonably well at estimating the wave height decay through the vegetation. This performance is quantitatively given in Table 2 for the four heterogeneous cases tested experimentally. Overall, the model-data agreement is very good, although there is a clear bias for the model to under-predict the wave height at the end of the high-density region, and slightly over-predict the wave height at the end of the vegetation. This error and bias can be the result of the inherent error in the empirical equations for friction factor, missing 2HD terms in these equations, or some neglected turbulent or vertically-varying physics not captured by the Boussinesq simulation. However, it is concluded that the empirical equations provide a reasonable estimate for friction factor due to vegetation, within the parameter range tested, and should be useful for numerous numerical simulation applications.

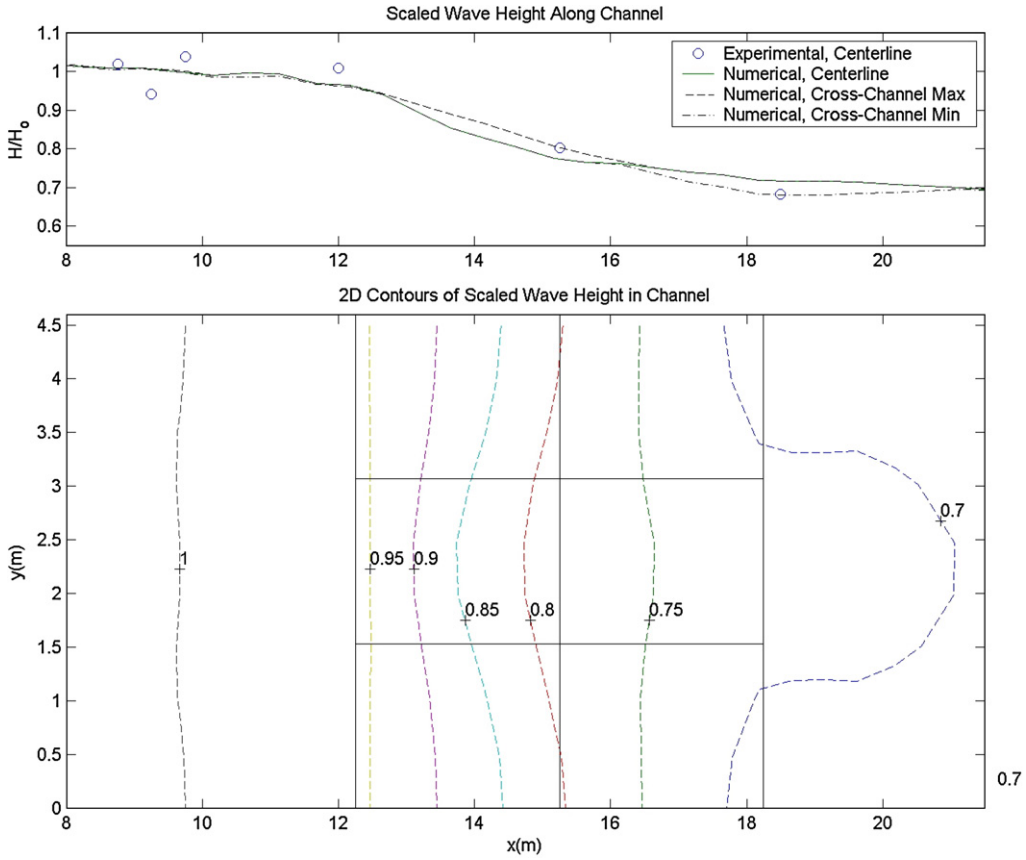

Fig. 9. Numerical results and experimental data for the heterogeneous vegetation case with H_{rms}=8.5 cm, T=2.0 s, and h=0.3 m. The top pane gives the wave height divided by the incident wave height along the centerline of the channel, and the bottom pane shows the plan-view contours of this scaled wave height as predicted by the numerical model. In the bottom pane, the dashed lines are lines of constant wave height.

7. Conclusions

The experiments showed that emergent conditions resulted in a higher amount of wave attenuation compared to near-emergent conditions. Emergent conditions are most prevalent in marsh and wetland systems during regular tidal conditions and during initial inundation by storm surge. Emergent conditions are expected to result in a higher amount of wave attenuation because the plant stem occupies the entire depth of the water column, unlike near-emergent conditions where the plant stem does not impede the top portion of the water column where orbital velocities are greatest. Near-emergent plant conditions are important when the wetland becomes inundated by storm surge, or in the case of subaquatic vegetation. The wave height decay followed the same trends for all the experimental cases and appeared to be most dependent on the ratio of stem length to water depth and stem density. Motion of the flexible elements is an important factor when considering the effects of plant rigidity on wave attenuation. However, the attenuation effects of the rigid and flexible vegetation elements appeared to be very similar in theses laboratory experiments and yielded the same friction factors.

Data analysis of drag coefficient using linear theory showed a higher dependence on Reynolds number during emergent conditions than during near-emergent conditions, while drag coefficients during near-emergent conditions exhibited somewhat higher correlation with the Keulegan–Carpenter number. This finding suggests a progressively weaker dependence between the drag coefficient and wave period as the ratio between plant stem height and water depth decreases.

The COULWAVE model was shown to accurately simulate the experimental cases using the friction factor approach. The values of the numerical friction factor for the conditions tested ranged between 0.05 and 0.19. Values were found to be primarily dependent on the height of the vegetation relative to the water depth. It was observed for near-emergent experiments, the friction factor increased with Ursell number. Modeling vegetation roughness through the use of a dimensionless friction factor was found to provide a reasonable estimate for the amount of wave attenuation that may occur through wetland marshes. The developed equations for both emergent and near-emergent plant conditions can be applied to estimate wave damping for practical engineering purposes if the vegetation stem density lies within the experimental range analyzed here, between 97 stems/m^2 and 194 stems/m^2, which are reasonable approximations for wetland plant species such as the commonly-occurring low marsh *S. alterniflora* plant species.

Acknowledgements

Support for this research was provided by Texas A&M University and the National Science Foundation (CBET-0427014). The authors would like to thank Dr. Billy Edge for allowing us to conduct these experiments in the Haynes Coastal Engineering Laboratory and Mr. John Reed, Mr. Oscar Cruz, Ms. Carmen Cruz, Mr. Gregery Balsmeier, and Mr. David Piazza for assisting with implementation and construction in the laboratory.

References

Asano, T., Deguchi, H., Kobayashi, N., 1992. Interaction between water waves and vegetation. Chapter 207, Proc. 23rd Intern. Coastal Eng. Conf., ASCE, vol. 3, pp. 2710–2723.
Bergen, A., Alderson, C., Bergfors, R., Aquila, C., Matsil, M.A., 2000. Restoration of *Spartina alterniflora* salt marsh following a fuel oil spill, New York City, NY. Wetland Ecol. Manag. 8, 185–195.
Camfield, F.E., 1983. Wind wave growth with high friction. J. Waterw., Port Coast. Ocean Eng. 109 (1), 115–117.
Dalrymple, R.A., Kirby, J.T., Hwang, P.A., 1984. Wave refraction due to areas of energy dissipation. J. Waterw., Port Coast. Ocean Eng. 110 (1), 67–79.
Dean, R.G., 1978. Effects of vegetation on shoreline erosional processes, wetland functions and values: the state of our understanding. Am. Water Resour. Assoc. 415–426.
Dean, R.G., Bender, C.J., 2006. Static wave setup with emphasis on damping effects by vegetation and bottom friction. Coast. Eng. 53, 149–156.
Dubi, A., Torum, A., 1995. Wave damping by kelp vegetation. Proc. 24th Intern. Coastal Eng. Conf., ASCE, pp. 142–156.
Elgar, S., Guza, R.T., 1985. Observations of bispectra of shoaling surface gravity waves. J. Fluid Mech. 161, 425–448.
Feagin, R., 2008. Personal communications.
Goring, D.G., 1978. Tsunamis—the propagation of long waves onto a shelf. Rep. KH-R-38. California Institute of Technology.
Kadlec, R.H., 1990. Overland flow in wetlands: vegetation resistance. J. Hydraul. Eng. 116, 691–707.
Kobayashi, N., Raichlen, A.W., Asano, T., 1993. Wave attenuation by vegetation. J. Waterw., Port Coast. Ocean Eng. 199 (1), 30–48.
Lima, S.F., Neves, C.F., Rosauro, N.M.L., 2006. Damping of gravity waves by fields of flexible vegetation. Proc. 30th Intern. Coast. Eng. Conf., vol. 1, pp. 491–503.
Liu, P.L.-F., Yoon, S.B., Kirby, J.T., 1985. Nonlinear refraction–diffraction of waves in shallow water. J. Fluid Mech. 153, 184–201.
Lynett, P., Wu, T.-R., Liu, P.L.-F., 2002. Modeling wave runup with depth-integrated equations. Coast. Eng. 46 (2), 89–107.
Mendez, F.J., Losada, I.J., 2004. An empirical model to estimate the propagation of random breaking and nonbreaking waves over vegetation fields. Coast. Eng. 51, 103–118.
Mendez, F.J., Losada, I.J., Losada, M.A., 1999. Hydrodynamics induced by wind waves in a vegetation field. J. Geophys. Res. 104 (C8), 18383–18396.
Mork, M., 1996. Wave attenuation due to bottom vegetation. Waves and Nonlinear Processes in Hydrodynamics. Kluwer Academic Publishers, pp. 371–382.
Munson, B.R., Okiishi, T.H., Young, D.F., 2002. Fundamentals of Fluid Mechanics, 4th ed. John Wiley & Sons, Inc.
Nepf, H.M., 2004. Vegetated flow dynamics. In: Fagherazzi, S., Marani, M., Blum, L. (Eds.), Ecogeomorphology of Tidal Marshes, Coastal and Estuarine Studies, vol. 59, pp. 137–164.
Price, W.A., Tomlinson, K.W., Hunt, J.N., 1968. The effect of artificial seaweed in promoting the build-up of beaches. Proc. 11th Intern. Coast. Eng. Conf., vol. 1, pp. 570–578.
Tiner, R.W., 1993. Field Guide to Coastal Wetland Plants of the Southeastern United States. The University of Massachusetts Press, Amherst, MA, pp. 80–83.
Tyler, A.C., Zieman, J.C., 1999. Patterns of development in the creekbank region of a barrier island *Spartina alterniflora* marsh. Mar. Ecol., Prog. Ser. 180, 161–177.
U.S. Department of Agriculture, 2008. Plants database. Natural Resources Conservation Service. http://plants.usda.gov/.
U.S. Environmental Protection Agency, America's Wetlands, 16 July 2007, <http://www.epa.gov/OWOW/wetlands/vital/toc.html>.
Wei, G., Kirby, J.T., Grilli, S.T., Subramanya, R., 1995. A fully nonlinear Boussinesq model for surface waves. I. Highly nonlinear, unsteady waves. J. Fluid Mech. 294, 71–92.